Chapter 18
Steady Motion of a Belt in Frictional Contact with a Rotating Pulley

Jakob Scheidl and Yury Vetyukov

Abstract The steady-state motion of belt drives is studied extensively in the literature. While traditional models rely on the theory of an extensible string, we aim to take bending effects into account. In this regard, it is well known that concentrated contact forces at the points of first and last contact with a pulley arise if shear deformations are restricted. To circumvent this issue, we utilise a shear deformable, Cosserat theory of rods. In particular, we study the contour motion of a belt that is transported over a single, rigid pulley with zones of stick, sliding friction and no contact. The Coulomb friction law governs the contact between the belt and the pulley. We present a novel finite element model that allows to obtain the steady-state solution directly. Furthermore, we deduce the corresponding closed boundary value problem and integrate it numerically. Results obtained for a particular parameter set demonstrate correspondence of the two approaches.

18.1 Problem Statement

We seek the steady-state motion of the belt segment depicted in Fig. 18.1. The domain of interest is enclosed by the two clamping positions, one on either side. The belt is transported from left to right, entering and leaving the interval $x \in [-L_x/2,\ L_x/2]$ with a constant mass transport rate $c = 1$.[1]

A circular, rigid pulley with radius $R = 0.7$ is placed symmetrically in between the borders and its centre is shifted by $H = -0.575$ in vertical direction j. The material length in the control volume L_s equals the distance between the clamping positions $L_x = L_s = 1$. The belt is made of linear elastic material with modulus $E = 5 \times 10^7$ and Poisson ratio $\nu = 0.45$. It has a rectangular cross section with thickness $h = 0.05$ and width $w = 0.1$. We assume Coulomb friction between belt

[1] The SI-system of units is used throughout the paper.

J. Scheidl (✉) · Y. Vetyukov
Institute of Mechanics and Mechatronics, TU Wien, Getreidemarkt 9/E325, 1060 Wien, Austria
e-mail: Jakob.Scheidl@tuwien.ac.at

H. Irschik et al. (eds.), *Dynamics and Control of Advanced Structures and Machines*,
Advanced Structured Materials 156,
https://doi.org/10.1007/978-3-030-79325-8_18

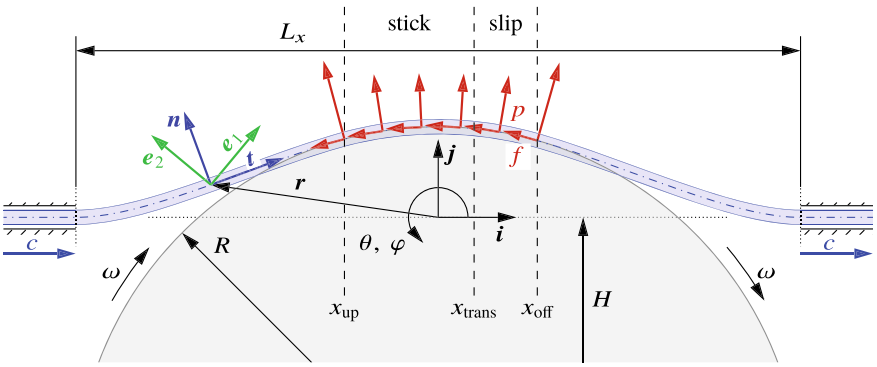

Fig. 18.1 One-pulley belt drive at contour motion; geometry and global coordinates

and pulley with the coefficient $\mu = 0.2$. In this respect, the belt's thickness is assumed to be small enough, such that we consider the contact reaction forces being applied at the middle line of the belt. Consequently, any distributed moments that would arise due to tractions acting on the lower fibre are disregarded. Inertia effects are ignored as well. Assuming that a solution with only one sticking and one sliding region exists, the latter succeeding the former in direction of travel, we explicitly set the position of the point where switching from stick to slip happens by means of x_{trans}. Admittedly, it would have been more natural to specify the angular velocity ω instead. However, in this academic example provision of x_{trans} is equally feasible and even proves beneficial with reasons to be given at the end of Sect. 18.4. The belt is modelled as a Cosserat elastic rod with bending stiffness a, extensional stiffness b_1 and shear stiffness b_2:

$$a = \frac{E\,h^3\,w}{12}\,, \quad b_1 = E\,h\,w\,, \quad b_2 = \frac{E}{2\,(1+\nu)}\,h\,w\,. \tag{18.1}$$

Incorporating shear deformability is essential to avoid concentrated contact interactions at the run-up- and the run-off-point, which are marked with x_{up} and x_{off} in Fig. 18.1, see [4].

In the usual Lagrangian kinematic setting, the actual configuration is described by the position vector r as a function of the material arc coordinate $r = r\,(s)$. The tangential unit vector t and the corresponding normal vector n are parametrised with an angle φ, which is measured against i,

$$t = \partial_s r/\,|\partial_s r| = i\,\cos\varphi + j\,\sin\varphi\,, \quad n = -i\,\sin\varphi + j\,\cos\varphi\,, \tag{18.2}$$

where we have used the acronym $\partial_s(\ldots) = \partial(\ldots)/\partial s$ to denote the material derivative. It is natural to describe the contact forces in this vector basis. The second system

$$e_1 = i\,\cos\theta + j\,\sin\theta\,, \quad e_2 = -i\,\sin\theta + j\,\cos\theta\,, \tag{18.3}$$

grasps the rotation of a material point by an angle θ, again measured against i. In the sense of a Timoshenko like theory, the vector e_1 points in normal direction of the deformed cross section. Thus, the shear deformation angle follows as

$$\psi = \theta - \varphi \,. \tag{18.4}$$

The undeformed state is assumed to be a straight line ($r_0 = x\, i$) and we refer to [1] for an example of a looped belt with a circular reference configuration.

The generalised force resultants M and Q are related to the deformations through the constitutive law, again see [1],

$$M = a\,\kappa \,, \quad Q = Q_1\, e_1 + Q_2\, e_2 = b_1\, \varepsilon\, e_1 + b_2\, \Gamma\, e_2 \,, \tag{18.5}$$

where κ is the bending strain measure; ε and Γ are the conjugate strain measures of the force components Q_1 and Q_2. The strains are related to the deformations through

$$\kappa = \partial_s \theta \,, \quad \varepsilon = (D\, \cos\psi - 1) \,, \quad \Gamma = -\,(D\, \sin\psi) \,, \quad D = |\partial_s r| \,, \tag{18.6}$$

and in absence of shear deformation ($\psi = 0$) the axial strain ε corresponds to the stretch D.

We use a dot to designate time derivatives and utilise the stationary material transport rate c to introduce an appropriate coordinate transformation:

$$s = s\,(\sigma,\, t) = \sigma - c\, t \,, \quad \partial_s \sigma = 1 \,, \quad \dot{\sigma} = c \,, \tag{18.7}$$

where the last equation holds due to $\dot{s} = 0$. Rewriting the governing equations in the new coordinate σ by simply replacing ∂_s with ∂_σ effectively eliminates the time dependence of field variables.

18.2 Finite Element Formulation

One way to obtain the contour motion of the belt is to seek stationary points of the total potential energy Π:

$$\delta\Pi = \delta U + \delta V = 0 \,, \tag{18.8}$$

where we have introduced the elastic strain energy U and the potential of contact forces V. These energy contributions may be written as line integrals over σ:

$$U = \int_{L_s} \left(\frac{1}{2}\, a\, \kappa^2 + \frac{1}{2}\, b_1\, \varepsilon^2 + \frac{1}{2}\, b_2\, \Gamma^2 \right) \mathrm{d}\sigma \,, \tag{18.9}$$

$$V = \int_{L_s} \left(\frac{1}{2}\, P_\mathrm{p}\, \gamma^2 + \lambda_\mathrm{p}\, \gamma \right) \mathrm{d}\sigma + \int_{L_s} (-\lambda_\mathrm{f}\, t \cdot r)\, \mathrm{d}\sigma \,. \tag{18.10}$$

The strain energy is a simple quadratic form featuring couples of stiffness coefficients and squared strain components. The contact potential is more complicated and deserves an in-depth discussion: It is divided into two separate integrals, the first one dealing with the contributions attributed to the normal contact pressure p and the second one with those related to the frictional force f. The strategy to compute the contact forces in the finite element framework is known as augmented Lagrangian method [3]. It features a penalty regularisation with penalty factors such as P_p and combines it with an iterative update of Lagrangian multiplier estimates such as λ_p and λ_f. Upon convergence of the iteration process, the penalty contributions vanish and only the Lagrangian multipliers persist.

Concerning the normal contact, the main kinematic condition to enforce is that the belt must not penetrate the pulley surface. We release this rigidity constraint and aim to fulfil it approximately by penalising any penetration γ, defined as

$$\gamma = \max\left(0,\ R - |r - H\,j|\right) \geq 0\,. \tag{18.11}$$

The first quadratic term in (18.10) is further augmented with the actual Lagrangian multiplier estimate λ_p, which is updated iteratively:

$$\lambda_\mathrm{p} \leftarrow \lambda_\mathrm{p} + P_\mathrm{p}\,\gamma\,. \tag{18.12}$$

Basically, the penalty contribution of the previous step is simply transferred to the Lagrange multiplier, improving the estimate and thereby reducing the penetration γ in the upcoming step.

The key condition for the frictional contact is that one must prevent any relative motion in the sticking part of the contact region. The velocity of a material point follows as the time derivative of the position vector:

$$v = \dot{r} = \partial_\sigma r\,\dot{\sigma} = c\,\partial_\sigma r = c\,D\,t\,. \tag{18.13}$$

The absolute value of a point's relative sliding velocity is

$$v_\mathrm{rel} = c\,D - R\,\omega\,. \tag{18.14}$$

Since ω is considered unknown, we cannot fulfil $v_\mathrm{rel} = 0$ directly, but have to demand $\partial_\sigma v_\mathrm{rel} = 0$ instead, which translates to

$$\partial_\sigma D = 0 \quad \Rightarrow \quad D = \bar{D} = \mathrm{const}\,. \tag{18.15}$$

The stretch in the sticking region $\bar{D}$ is constant. The original condition $v_\mathrm{rel} = 0$ now serves as an equation to calculate the corresponding value of ω. As the transition position x_trans is provided explicitly, the zones of stick and slip are known in advance and the frictional tractions can be assigned directly:

$$x < x_\mathrm{trans}:\ \lambda_\mathrm{f} \leftarrow P_\mathrm{f}\,\partial_\sigma D + \lambda_\mathrm{f}\,, \quad x \geq x_\mathrm{trans}:\ \lambda_\mathrm{f} \leftarrow -\mu\,\lambda_\mathrm{p}\,, \tag{18.16}$$

with P_f denoting the penalty factor for sticking contact. The negative sign in front of μ indicates forward sliding of the belt.

The finite element formulation itself is based on a discretisation of the position vector r as well as the angle of particle rotation θ. Cubic shape functions are used to approximate the fields and their first derivatives in the local coordinate $\xi \in [-1,\ 1]$ of a single, two-node element. The integrals (18.9)–(18.10) are transformed to a sum of finite element contributions in the usual manner and evaluated by means of Gaussian quadrature rules with three integration points.

A pure Newton–Raphson algorithm is used to solve the non-linear system of equations. In order to obtain results more reliably, the solution process is split into two phases: Firstly, a frictionless solution with relaxed penalty for normal contact is sought, which counteracts the ill-conditioning induced through the penalty terms and simply disregards the second integral of (18.10). Secondly, the full penalty is applied and frictional forces are taken into account. A number of steps is performed in order to reach convergence of the Lagrange multiplier estimates. We resolve the contact state discretely at individual integration points and call the update routines (18.12) and (18.16) once after each successful Newton step. The size of the contact zone is determined by the first and last integration point for which contact is recognised.

18.3 Analytic Model

Just like in the finite element model, we assume the solution to decompose into four sequential segments: the left free span, the sticking region, the sliding region and the right free span. In an effort to deduce the system of differential equations we will address a single free span and the two contact segments individually, each time being mindful of the particularities:

- No external forces act in any of the two free span regions.
- In the sticking region the belt adheres to the pulley surface.
- In the sliding region the friction forces must obey the friction law.

The model is an extension of the idealised one presented in [2]. We have already provided the constitutive relations (18.5) and also given the definition of strains in (18.6), but we have yet to present the balance equations of the non-linear theory:

$$\partial_s Q + q = 0\,, \quad \partial_s M + D\ (Q_1\ \sin\psi + Q_2\ \cos\psi) = 0\,. \tag{18.17}$$

The vector of external forces vanishes in the free spans and otherwise equals the contact forces, $q = f\,t + p\,n$.

Once again, we make use of the coordinate transformation (18.7) to get rid of the time dependence of field variables and replace every single instance of ∂_s with ∂_σ in the governing system. Beyond that, it is convenient to introduce spatial coordinates like x or φ for each solution region with the main consequence that σ becomes an additional unknown:

$$\text{free span regions:} \quad \sigma = \sigma(x)\,, \quad \partial_\sigma = \partial_x / \partial_x \sigma\,, \quad r = x\,i + y(x)\,j\,, \tag{18.18}$$

$$\text{contact regions:} \quad \sigma = \sigma(\varphi)\,, \quad \partial_\sigma = \partial_\varphi / \partial_\varphi \sigma\,, \quad r = H\,j + R\,n(\varphi)\,. \tag{18.19}$$

Owing to the absence of external forces, the derivation of a system of ODEs in the free span region is quite simple. We obtain equations for σ and y through evaluation of $\partial_\sigma r = D\,t$ with the above transformation rule (18.18) and projection onto the Cartesian basis vectors. The constitutive relation (18.5) for M serves as an equation for θ and the ones for the force components are used for substitution in the balance of moments, which yields an ODE for M. Lastly, based on the balance of linear momentum, we derive equations for the stretch D and the shear angle ψ:

$$\begin{aligned}
&\partial_x \sigma = (D\,\cos\varphi)^{-1}\,, \quad \partial_x y = \tan\varphi\,, \quad \partial_x \theta = \partial_x \sigma\, M/a\,,\\
&\partial_x M = \partial_x \sigma \left(D^2\,\sin(2\,\psi)\,\frac{b_2 - b_1}{2} + D\,b_1\,\sin\psi \right),\\
&\partial_x D = \partial_x \theta \left(D\,\sin(2\,\psi)\,\frac{b_1^2 - b_2^2}{2\,b_1\,b_2} - \frac{b_1}{b_2}\,\sin\psi \right),\\
&\partial_x \psi = \partial_x \theta \left(\cos(2\,\psi)\,\frac{b_1^2 - b_2^2}{2\,b_1\,b_2} + \frac{b_1^2 + b_2^2}{2\,b_1\,b_2} - \frac{b_1}{b_2\,D}\,\cos\psi \right).
\end{aligned} \tag{18.20}$$

Treating the sticking region is more concise, because only three ODEs for $\{\sigma,\ \theta,\ M\}$ suffice. They resemble the ones given above, with the main differences that the unknown constant stretch $\bar{D}$ enters the equations and that φ is used for parametrisation instead of x:

$$\begin{aligned}
&\partial_\varphi \sigma = -R/\bar{D}\,, \quad \partial_\varphi \theta = \partial_\varphi \sigma\, M/a\,,\\
&\partial_\varphi M = \partial_\varphi \sigma \left(\bar{D}^2\,\sin(2\,\psi)\,\frac{b_2 - b_1}{2} + \bar{D}\,b_1\,\sin\psi \right).
\end{aligned} \tag{18.21}$$

The above three equations also apply to the sliding region, once the constant $\bar{D}$ is replaced with the variable $D = D(\varphi)$. Consequently, another equation for the stretch is needed, whose deduction is more tedious as it requires substitution of the friction criterion $f = -\mu\,p$ in the balance of forces:

$$\begin{aligned}
\partial_\varphi D = {} & \frac{D\,\left(2\,\partial_\varphi \theta - 1\right)\,(b_1 - b_2)\,\left(\mu\,\cos(2\,\psi) + \sin(2\,\psi)\right)}{(b_1 - b_2)\,\left(\cos(2\,\psi) - \mu\,\sin(2\,\psi)\right) + b_1 + b_2}\\
& + \frac{\mu\,D\,(b_1 + b_2) - 2\,\partial_\varphi \theta\, b_1\,\left(\mu\,\cos\psi + \sin\psi\right)}{(b_1 - b_2)\,\left(\cos(2\,\psi) - \mu\,\sin(2\,\psi)\right) + b_1 + b_2}\,.
\end{aligned} \tag{18.22}$$

This concludes the system with a total of nineteen ODEs: two times six for the free spans, three for the sticking region and four for the sliding region. Boundary conditions at $x = \pm L_x/2$ demand continuity of σ, the vertical deflection and the particle rotation ($\sigma = \pm L_x/2,\ y = 0,\ \theta = 0$). In general, the shear deformation ψ will not vanish at these points and the beam axis will thus experience a slight kink.

Matching conditions have to be employed at the run-up- and the run-off-point (x_{up} and x_{off} in Fig. 18.1). There, we demand continuity of all six unknowns that appear in the system (18.20). Lastly, at the transition point x_{trans}, we require continuity of $\{\sigma,\ \theta,\ M,\ D\}$. These are a total of 22 boundary conditions for 19 first order ODEs and three unknown constants, namely: The points x_{up} and x_{off} as well as the constant stretch in the sticking region $\bar{D}$. Before passing the system to the Matlab collocation solver bvp4c, we further transform the equations to a normalised coordinate $\xi \in [0,\ 1]$, see [1, 4], and introduce dimensionless constants to reduce the number of parameters.

18.4 Results

Let us take a look at the contact forces in Fig. 18.2 and at the strains in Fig. 18.3. Plots are drawn for the results obtained through integration of the boundary value problem (BVP, dotted) as well as for a finite element simulation with 100 equally sized elements (FEM, dashed). Though both approaches converge rapidly, the FEM simulation requires a higher computational effort owing to the two-stage iterative solution strategy and the number of elements needed to reach accurate results. The transition point is set to $x_{\text{trans}} = 0$ and the contact zone borders x_{up} and x_{off} are marked with additional vertical grid lines.

In Fig. 18.2, the normal contact pressure p shows distinct peaks at the points x_{up} and x_{off}. Contrary to unshearable rod theories though, the function does not tend to infinity. The frictional tractions experience corresponding peaks as well as a jump at the transition point $x_{\text{trans}} = 0$ in obedience to the friction law. The coarse discretisation does not suffice to capture the high gradients at the two bordering positions, which is most evident at x_{up} in the right picture of Fig. 18.2. This issue can be easily resolved by using more elements or an appropriately refined mesh.

Figure 18.3 depicts the distribution of the two force strain measures. The results obtained with 100 elements conform very well to the semi-analytic reference solution. The axial strains ε are constant in the sticking region, as demanded by (18.15), and gradually increase in the sliding zone. The peaks of the shear strain distribution on

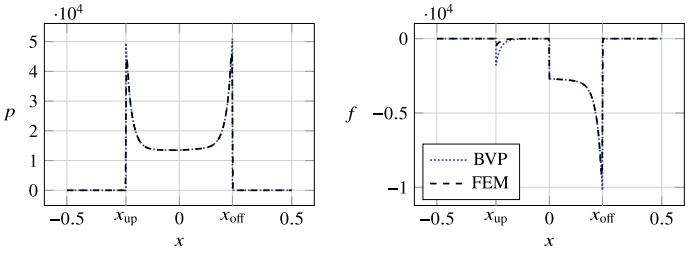

Fig. 18.2 Distributions of normal (left) and tangential contact forces (right)

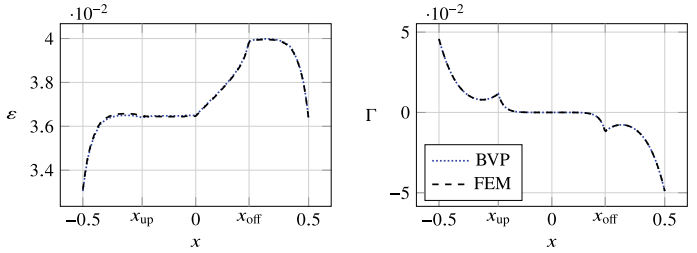

Fig. 18.3 Distributions of strain measures ε (left) and Γ (right)

the right are obviously related to the establishment and loss of contact and, aside from the bordering regions, no significant shear deformation arises in the contact domain. Different results are to be expected, once distributed contact moments come into play, which are absent here.

Demanding $v_{\text{rel}} = 0$ in (18.14) for $x_{\text{trans}} = 0$ yields an angular velocity of $\omega = 1.4807$ (the relative error between the models is less than 1×10^{-4}). Now, to estimate the range of meaningful values for ω, we can simply shift x_{trans} towards the bordering points x_{off} and x_{up} to find limiting solutions of a pure sticking and a pure sliding belt, respectively. The corresponding interval turns out to be extremely tight: $\omega \in [1.4779,\ 1.4825]$, which clearly demonstrates the advantage of providing x_{trans} as part of the system parameters instead of ω.

18.5 Conclusion

We have developed a finite element procedure to compute the stationary motion of the considered one-pulley belt drive example. The scheme relies on the theory of shear deformable rods, and the simulation results are compared to analytic results obtained through numerical integration of the corresponding boundary value problem.

To this end, only a single pulley has been considered and the closed loop, two-pulley belt drive problem is left for future research. Again, shear deformable rod theory should be used when tackling this more complex problem with the proposed solution strategies. For completeness, stationary dynamics should be considered as well. A difficulty that arises in the looped problem is that the constant material transport velocity c becomes an additional unknown.

References

1. Belyaev, A.K., Eliseev, V.V., Irschik, H., Oborin, E.A.: Dynamics of Contour Motion of Belt Drive by Means of Nonlinear Rod Approach, pp. 21–29. Springer International Publishing, Cham (2019). https://doi.org/10.1007/978-3-319-90884-7_3
2. Oborin, E., Vetyukov, Y.: Steady state motion of a shear deformable beam in contact with a traveling surface. Acta Mech. **230**(11), 4021–4033 (2019). https://doi.org/10.1007/s00707-019-02476-x
3. Simo, J., Laursen, T.: An augmented Lagrangian treatment of contact problems involving friction. Comput. Struct. **42**(1), 97–116 (1992). https://doi.org/10.1016/0045-7949(92)90540-G
4. Vetyukov, Y., Oborin, E., Scheidl, J., Krommer, M., Schmidrathner, C.: Flexible belt hanging on two pulleys: contact problem at non-material kinematic description. Int. J. Solids Struct. **168**, 183–193 (2019). https://doi.org/10.1016/j.ijsolstr.2019.03.034